across the junction is proportional to the product of the end-tunnelling density of states on both sides and therefore still varies as a power law of energy, but with an exponent twice as large as the end tunnelling, that is, $\alpha_{\text{end–end}} = 2\alpha_{\text{end}}$.

Single-wall carbon nanotubes are truly one-dimensional conductors and are thus expected to behave as LLs. The strength of electron interactions is described by the so-called Luttinger parameter g. For non-interacting electrons $g = 1$, whereas for repulsive Coulomb interactions $g < 1$. The exponents α for tunnelling into the bulk and end of a nanotube LL are related to g as $\alpha_{\text{bulk}} = (g^{-1} + g - 2)/8$ and $\alpha_{\text{end}} = (g^{-1} - 1)/4$ respectively[18]. In our experiments, bulk tunnelling is expected for the measurements of the straight segments. Fitting the high-temperature data for the two straight segments yields similar exponents $\alpha = 0.34$ and 0.35, which gives a value of $g \approx 0.22$ using the above expression for bulk tunnelling. This g value agrees with theoretical estimates[17,18] and with that reported for ropes[16] and clearly indicates the strong electron–electron interactions in SWNTs. Having established that both straight segments are LLs, we expect that the conduction process between the middle two contacts takes place via end-to-end tunnelling between the two LLs as well as tunnelling in and out of the two LLs through the contacts. However, the end-to-end tunnelling dominates the energy dependence of the process. Substituting the above g value into $\alpha_{\text{end–end}} = (g^{-1} - 1)/2$, an exponent of 1.8 is expected for the tunnelling conductance across the junction. Fitting the experimental data with a power law yields $\alpha = 2.2$, which is indeed close to this value. This analysis is not based on any presumed g value (which is sample-dependent). The self-consistency of bulk and end-to-end tunnelling thus provides strong evidence for the Luttinger model.

We have also measured large-bias I–V characteristics across the M–M junction at different temperatures, which provide an independent verification of the LL theory. As is evident from Fig. 4a, the I–V curves are nonlinear at all temperatures. The current is expected to increase as $V^{\alpha+1}$ for $eV \gg k_B T$. We consider the differential conductance which, assuming a constant tunnelling amplitude across the junction, is predicted to satisfy a scaling function:

$$\frac{dI}{dV} \propto T^{\alpha} \sinh\left(\frac{eV}{2k_B T}\right) \left| \Gamma\left(1 + \frac{\alpha}{2} + i\frac{eV}{2\pi k_B T}\right) \right|^2 \times \left\{ \frac{1}{2} \coth\left(\frac{eV}{2k_B T}\right) - \frac{1}{\pi} Im\left[\Psi\left(1 + \frac{\alpha}{2} + i\frac{eV}{2\pi k_B T}\right) \right] \right\}$$

Here α is the end-to-end tunnelling exponent and Γ and Ψ are the gamma and digamma functions respectively. For $\alpha = 2$, a good approximation (exact when $\alpha = 2$) of the above expression is given by $dI/dV \propto T^{\alpha}(1 + 3(eV/2\pi k_B T)^{\alpha})$, which clearly shows the expected power-law behaviour at large bias. The expression suggests that if we scale dI/dV by T^{α} and V by T, then curves obtained at different temperatures should all collapse onto one universal curve. This is shown in Fig. 4b for our experimental data. The scaled conductance is constant for small V but crosses over to a power law for $eV/k_B T > 3$. Its behaviour is qualitatively similar to the theoretical scaling function (dashed line) in Fig. 4b. The deviation at large bias may be explained by a reduced voltage drop and/or a reduced tunnelling amplitude across the kink (see Fig. 4 legend). Overall, however, end-to-end tunnelling between two LLs seems to capture the main physics of the observed data. □

Received 24 June; accepted 29 September 1999.

1. Wildöer, J. W. G., Venema, L. C., Rinzler, A. G., Smalley, R. E. & Dekker, C. Electronic structure of atomically resolved carbon nanotubes. *Nature* **391,** 59–62 (1998).
2. Odom, T. W., Huang, J., Kim, P. & Lieber, C. M. Atomic structure and electronic properties of single-walled carbon nanotubes. *Nature* **391,** 62–64 (1998).
3. Tans, S. J. *et al.* Individual single-wall carbon nanotubes as quantum wires. *Nature* **386,** 474–477 (1997).
4. Bockrath, M. *et al.* Single-electron transport in ropes of carbon nanotubes. *Science* **275,** 1922–1925 (1997).
5. Tans, S. J., Verschueren, A. R. M. & Dekker, C. Room-temperature transistor based on a single carbon nanotube. *Nature* **393,** 49–52 (1998).
6. Chico, L., Crespi, V. H., Benedict, L. X., Louie, S. G. & Cohen, M. L. Pure carbon nanoscale devices: Nanotube heterojunctions. *Phys. Rev. Lett.* **76,** 971–974 (1996).
7. Lambin, Ph., Fonseca, A., Vigneron, J. P., Nagy, J. B. & Lucas, A. A. Structural and electronic properties of bent carbon nanotubes. *Chem. Phys. Lett.* **245,** 85–89 (1995).
8. Saito, R., Dresselhaus, G. & Dresselhaus, M. S. Tunnelling conductance of connected carbon nanotubes. *Phys. Rev. B* **53,** 2044–2050 (1996).
9. Charlier, J.-C., Ebbesen, T. W. & Lambin, Ph. Structural and electronic properties of pentagon-heptagon pair defects in carbon nanotubes. *Phys. Rev. B* **53,** 11108–11113 (1996).
10. Menon, M. & Srivastava, D. Carbon nanotube "T junctions": Nanoscale metal-semiconductor-metal contact devices. *Phys. Rev. Lett.* **79,** 4453–4456 (1997).
11. Chico, L., López Sancho, M. P. & Muñoz, M. C. Carbon-nanotube-based quantum dot. *Phys. Rev. Lett.* **81,** 1278–1281 (1998).
12. Iijima, S., Brabec, C. J., Maiti, A. & Bernholc, J. Structural flexibility of carbon nanotubes. *J. Chem. Phys.* **104,** 2089–2092 (1996).
13. Yakobson, B. I., Brabec, C. J. & Bernholc, J. Nanomechanics of carbon tubes: Instabilities beyond the linear response. *Phys. Rev. Lett.* **76,** 2511–2514 (1996).
14. Collins, P. G., Zettl, A., Bando, H., Thess, A. & Smalley, R. E. Nanotube nanodevice. *Science* **278,** 100–103 (1997).
15. Chico, L., Benedict, L. X., Louie, S. G. & Cohen, M. L. Quantum conductance of carbon nanotubes with defects. *Phys. Rev. B* **54,** 2600–2606 (1996).
16. Bockrath, M. *et al.* Luttinger-liquid behaviour in carbon nanotubes. *Nature* **397,** 598–601 (1999).
17. Egger, R. & Gogolin, A. Effective low-energy theory for correlated carbon nanotubes. *Phys. Rev. Lett.* **79,** 5082–5085 (1997).
18. Kane, C., Balents, L. & Fisher, M. P. A. Coulomb interactions and mesoscopic effects in carbon nanotubes. *Phys. Rev. Lett.* **79,** 5086–5089 (1997).
19. Fisher, M. P. A. & Glazman, L. I. in *Mesoscopic Electron Transport* (eds Kouwenhoven, L. P., Sohn, L. L. & Schön, G.) 331–373 (Kluwer Academic, Boston, 1997).

Supplementary information is available on *Nature*'s World-Wide Web site (http://www.nature.com) or as paper copy from the London editorial office of *Nature*.

Acknowledgements

We thank R. E. Smalley and co-workers for providing the indispensable single-wall carbon nanotube materials, M. P. Anantram, S. J. Tans and A. A. Odintsov for helpful discussions, V. Meunier for the atomic coordinates used in Fig. 1c, and M. de Jonge and A. van den Enden for experimental assistance. The work was supported by the Dutch Foundation for Fundamental Research on Matter (FOM).

Correspondence and requests for materials should be addressed to C.D. (e-mail: dekker@qt.tn.tudelft.nl).

Design and synthesis of an exceptionally stable and highly porous metal-organic framework

Hailian Li*, Mohamed Eddaoudi†, M. O'Keeffe* & O. M. Yaghi†

*Materials Design and Discovery Group, * Department of Chemistry and Biochemistry, Arizona State University, Tempe, Arizona 85287-1604, USA*
† Department of Chemistry, University of Michigan, 930 North University, Ann Arbor, Michigan 48109-1055, USA

Open metal–organic frameworks are widely regarded as promising materials for applications[1–15] in catalysis, separation, gas storage and molecular recognition. Compared to conventionally used microporous inorganic materials such as zeolites, these organic structures have the potential for more flexible rational design, through control of the architecture and functionalization of the pores. So far, the inability of these open frameworks to support permanent porosity and to avoid collapsing in the absence of guest molecules, such as solvents, has hindered further progress in the field[14,15]. Here we report the synthesis of a metal–organic framework which remains crystalline, as evidenced by X-ray single-crystal analyses, and stable when fully desolvated and when heated up to 300 °C. This synthesis is achieved by borrowing ideas from metal carboxylate cluster chemistry, where an organic

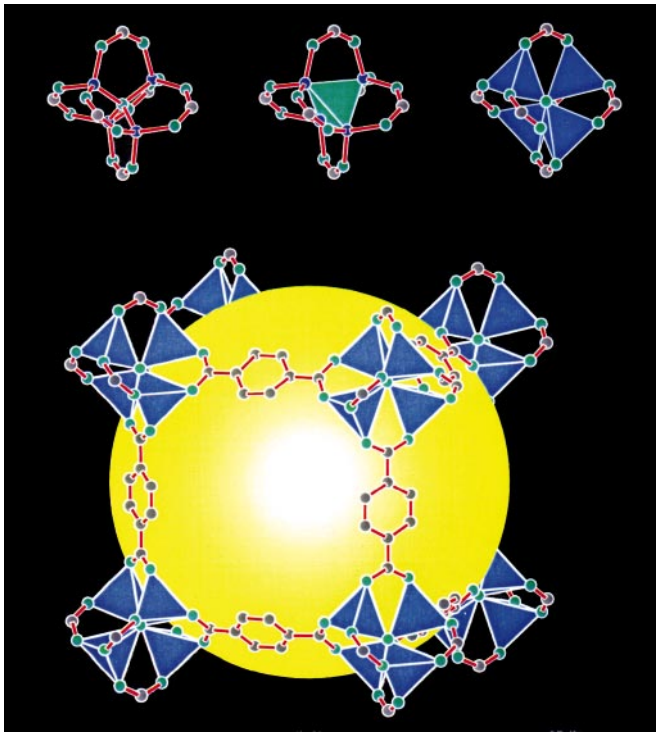

Figure 1 Construction of the MOF-5 framework. Top, the $Zn_4(O)O_{12}C_6$ cluster. Left, as a ball and stick model (Zn, blue; O, green; C, grey). Middle, the same with the $Zn_4(O)$ tetrahedron indicated in green. Right, the same but now with the ZnO_4 tetrahedra indicated in blue. Bottom, one of the cavities in the $Zn_4(O)(BDC)_3$, MOF-5, framework. Eight clusters (only seven visible) constitute a unit cell and enclose a large cavity, indicated by a yellow sphere of diameter 18.5 Å in contact with 72 C atoms (grey).

dicarboxylate linker is used in a reaction that gives supertetrahedron clusters when capped with monocarboxylates. The rigid and divergent character of the added linker allows the articulation of the clusters into a three-dimensional framework resulting in a structure with higher apparent surface area and pore volume than most porous crystalline zeolites. This simple and potentially universal design strategy is currently being pursued in the synthesis of new phases and composites, and for gas-storage applications.

The tetranuclear supertetrahedral cluster motif shown in Fig. 1a is adopted by a number of metal carboxylates (acetate, benzoate and pivalate), where combination of Zn^{2+} and the appropriate carboxylic acid yields the oxide centred cluster as a distinct and well-defined unit[16]. Working towards an extended network based on this cluster, we viewed its Zn–O–C motif as a secondary building unit capable of assembly under similar reaction conditions but in the presence of a dicarboxylate instead of a monocarboxylate. Our earlier work[18] involving the copolymerization of 1,4-benzenedicarboxylate (BDC) with metal ions pointed to its rigid, planar, and divergent attributes, which, when coupled with the rigidity of this secondary building unit, would be ideally suited in forming the target extended three-dimensional framework shown in Fig. 1b.

We found that diffusion of triethylamine into a solution of zinc (II) nitrate and H_2BDC in *N*,*N*′-dimethylformamide (DMF)/chlorobenzene resulted in the deprotonation of H_2BDC and its reaction with Zn^{2+} ions. A small amount of hydrogen peroxide was added to the reaction mixture in order to facilitate the formation of O^{2-} expected at the centre of the secondary building unit. Elemental microanalysis of the resulting colourless cubic crystals suggested that their formula was $Zn_4O(BDC)_3{\cdot}(DMF)_8(C_6H_5Cl)$; here we call this material MOF-5, where MOF indicates metal organic framework. The presence of DMF and chlorobenzene guests was confirmed by solid-state ^{13}C NMR, which showed sharp characteristic peaks at the chemical shifts expected for the carbon atom resonances of these guests. Ion mass spectrometry, performed on the liberated guest vapours as the material was heated from 22 to 350 °C, showed their respective parent-ion masses.

An X-ray single-crystal diffraction study on the as-synthesized materials reveals the expected topology (Fig. 2). The structure may be derived from a simple cubic six-connected net in two stages: first, the nodes (vertices) of the net are replaced by clusters of secondary building units; second, the links (edges) of the net are replaced by finite rods ('struts') of BDC molecules. The core of the cluster

Table 1 Gas and liquid vapour sorption in desolvated MOF-5

Sorbate	*T* (°C)	Amount sorbed ($mg\,g^{-1}$)	Sorbate molecules per unit cell	Free volume ($cm^3\,g^{-1}$)	Free volume ($cm^3\,cm^{-3}$)
Ar	–194	1,492	230	1.03	0.61
N_2	–194	831	183	1.04	0.61
CH_2Cl_2	22	1,211	88	0.93	0.55
$CHCl_3$	22	1,367	71	0.94	0.55
C_6H_6	22	802	63	0.94	0.55
CCl_4	22	1,472	59	0.94	0.56
C_6H_{12}	22	703	51	0.92	0.54

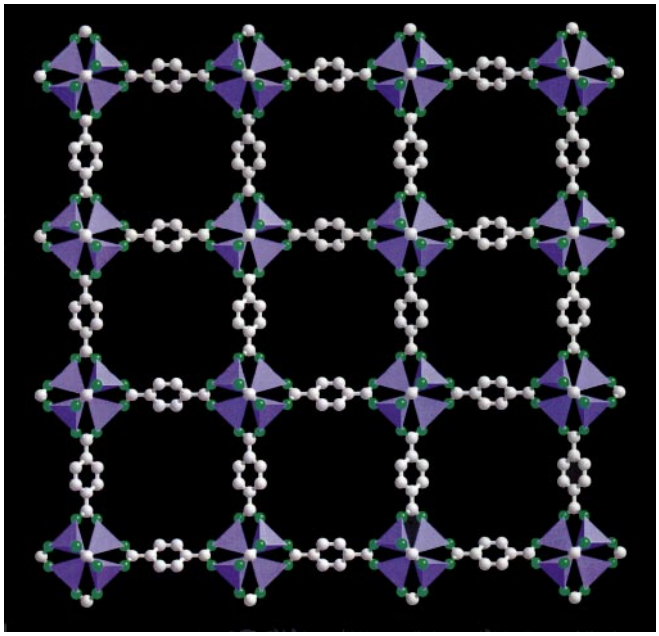

Figure 2 Representation of a {100} layer of the MOF-5 framework shown along the *a*-axis (C, grey; O, green). The ZnO_4 tetrahedra are indicated in purple. Properties of MOF-5 are as follows. Single crystals of as-synthesized $Zn_4O(BDC)_3{\cdot}(DMF)_8(C_6H_5Cl)$, MOF-5, are at 213 ± 2 K cubic, space group *Fm*-3*m* with $a = 25.6690(3)$ Å, $V = 16{,}913.2(3)$ Å, and $Z = 8$. Analysis for MOF-5. (1) Elemental microanalysis. Calculated (%); C, 44.21; H, 5.02; N, 7.64; Zn, 17.82%. Found (%): C, 43.25; H, 5.29; N, 7.56; Zn, 17.04%. (2) Solid-state ^{13}C NMR. First, CP MAS. Guests $(CH_3)_2NC(O)H$: $(CH_3)_2$-, δ (p.p.m.) 37.81 and 32.71; -C(O)-, δ 164.93. C_6H_5Cl: δ 132.04, 130.41, 128.76. Framework, –COO, δ 175.93; –C(COO), δ 139.11; *o*-C_6H_4, δ 130.41. Second, static. Guests $(CH_3)_2NC(O)H$: $(CH_3)_2$-, δ 37.63 and 32.59; -C(O)-, δ 164.67. C_6H_5Cl: δ 130.22 (broad). Framework, no peaks observed. (3) Mass spectrometry, 22–350 °C. $(CH_3)_2NC(O)H$: M^+, 73 a.m.u. ($C_3H_7NO^+$). C_6H_5Cl: M^+, 77 ($C_6H_5^+$); M^+, 112 a.m.u. ($C_6H_5{}^{35}Cl^+$) and 114 a.m.u. ($C_6H_5{}^{37}C^+$) in 3:1 intensity ratio. Properties of single crystals of fully desolvated MOF-5, $Zn_4O(BDC)_3$, are at 169 ± 2 K cubic, space group *Fm*-3*m* with $a = 25.8849(3)$ Å, $V = 17{,}343.6(8)$ Å^3, and $Z = 8$ (for empirical formula, $C_{24}H_{12}O_{13}Zn_4$), R, $R_w = 0.023$, 0.026. Analysis for $Zn_4O(BDC)_3$. Elemental microanalysis. Calculated (%): C, 37.45; H, 1.57; N, 0.00%. Found (%): C, 36.94; H, 1.66; N, 0.26%. Solid-state ^{13}C NMR (CP MAS and static) showed no resonances due to any guests. Mass spectrometry (22–350 °C) showed no peaks, indicative of absence of any guests in the pores. Thermogravimetric analysis showed no weight loss up to 410 °C. Single crystals of $Zn_4O(BDC)_3$, fully desolvated and heated at 300 °C, are at 149 ± 2 K cubic, space group *Fm*-3*m* with $a = 25.8496(3)$ Å.

consists of a single O atom bonded to four Zn atoms, forming a regular Zn_4O tetrahedron. Each edge of each Zn tetrahedron is then capped by a $-CO_2$ group to form a $Zn_4(O)(CO_2)_6$ cluster. We note that a related zinc phosphate structure exists[17], in which the C atoms are replaced by the P atoms of PO_4 tetrahedra, which serves to link the clusters together. The important step taken in the present work is the replacement of the O_2–P–O_2 phosphate links by O_2–C–C_6H_4–C–O_2 (BDC) 'struts', to give an extended network having a three-dimensional intersecting channel system with 12.94-Å spacing between the centres of adjacent clusters.

The framework atoms in MOF-5 take up only a small fraction of the available space in the crystal. If overlapping spheres with van der Waals radii (1.5, 1.2, 1.7, 1.5 Å for Zn, H, C and O, respectively) are placed at the atomic positions, the space not so occupied is 80% of

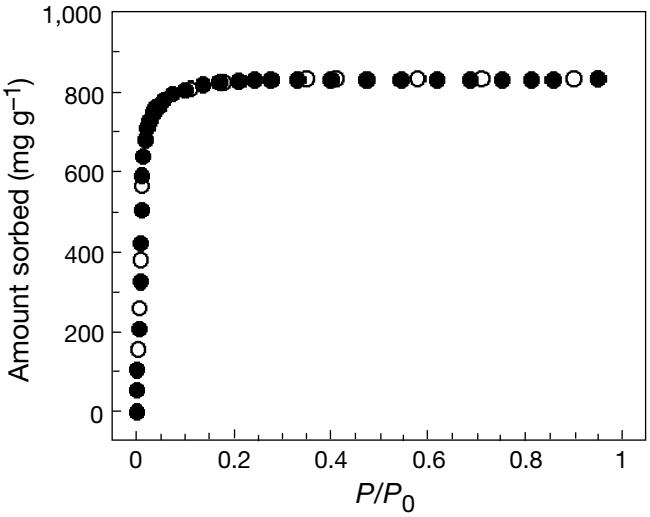

Figure 3 Nitrogen gas sorption isotherm at 78 K for MOF-5 (filled circles, sorption; open circles desorption). P/P_0 is the ratio of gas pressure (P) to saturation pressure (P_0), with $P_0 = 746$ torr.

the crystal volume. The non-framework space is divided into two types of cavity lined with C and H atoms. The centre of the smaller of these has 24 H atoms at 7.10 Å and 24 C atoms at 7.97 Å; the centre of the larger (Fig. 1) has 72 C atoms at 9.26 Å and 48 H atoms at 9.47 Å. The aperture joining the two cavities has 8 H at 5.10 Å and 8 C at 5.70 Å from its centre. Allowing for the van der Waals radii, spheres of material with diameter 15.1 Å and 11.0 Å could fit in the large and small cavities, respectively, and the aperture would admit the passage of a sphere of diameter 8.0 Å. Assuming the same molar volume as in the respective liquids, we find that in the original material the guest molecules—$8 \times (8\,\mathrm{DMF} + 1\,C_6H_5Cl)$—have a volume of 9,512 $Å^3$, which is 55% of the unit cell volume. Indeed, we show below that 55–61% of the space is accessible to guest species.

Due to their high mobility, the guests can be fully exchanged with chloroform. More significant is that all the chloroform guests can be evacuated from the pores within 3 h at room temperature and 5×10^{-5} torr without loss of framework periodicity. In fact, the desolvated single crystals were checked by elemental microanalysis, ^{13}C NMR, mass spectrometry, and thermal gravimetry to confirm the absence of any guests, while optical microscopy was used to show that they maintained their transparency, morphology and crystallinity. This has allowed us to perform another X-ray single-crystal diffraction study on the fully desolvated form of this framework—a study that revealed mono-crystallinity with cell parameters and atomic positions coincident with those of the as-synthesized material. In fact, the highest peaks and lowest valleys in the ΔF map are 0.25 and −0.17 electrons per $Å^3$ scattered randomly both near the framework and the void space. These contrast with the relatively large values (1.56 and −0.45 electrons per $Å^3$) found in the as-synthesized crystals.

Further evidence for the stability of the framework was obtained by heating the fully desolvated crystals in air at 300 °C for 24 h, which had no effect on either their morphology or crystallinity as evidence by another X-ray single-crystal diffraction study. Here again, the cell parameters obtained were unaltered relative to those found for the unheated desolvated crystals, illustrating the rigidity and stability of the framework in the absence of guest molecules. These results are interesting as the density ($0.59\,g\,cm^{-3}$) of the desolvated crystals is among the lowest recorded for any crystalline material.

To evaluate the pore volume and the apparent surface area of this framework, the gas and vapour sorption isotherms for the desolvated sample were measured using an electromicrogravimetric balance (Cahn 1000) set-up and an already published procedure[18]. The sorption of nitrogen revealed a reversible type I isotherm (Fig. 3), with concordant results obtained with large crystals (0.2 mm) and microcrystals (30 μm). The same sorption behaviour was observed for argon and organic vapours such as CH_2Cl_2, $CHCl_3$, CCl_4, C_6H_6 and C_6H_{12}. Similar to those of most zeolites, the isotherms are reversible and show no hysteresis upon desorption of gases from the pores. Using the Dubinin–Raduskhvich equation, pore volumes of 0.61–0.54 $cm^3\,cm^{-3}$ were calculated and found to be nearly identical for all adsorbates shown (Table 1), which indicates the presence of uniform pores. Assuming a monolayer coverage of N_2 (which may not be strictly correct with such large cavities) the apparent Langmuir surface area was estimated at 2,900 $m^2\,g^{-1}$. Zeolites, which generally have higher molar masses than $Zn_4O(BDC)_3$, have pore volumes that range from 0.18 $cm^3\,cm^{-3}$ for analcime to 0.47 $cm^3\,cm^{-3}$ for zeolite A[19]. □

Received 20 May; accepted 17 September 1999.

1. Kinoshita, Y., Matsubara, I., Higuchi, T. & Saito, Y. The crystal structure of bis(adiponitrilo) copper(I) nitrate. *Bull. Chem. Soc. Jpn* **32,** 1221–1226 (1959).
2. Kitgawa, S., Munakata, M. & Tanimura, T. Tetranuclear copper(I)-based infinite one-dimensional chain complex. *Chem. Lett.* 623–626 (1991).
3. Abrahams, B. F., Hoskins, B. F. & Robson, R. Infinite polymeric frameworks consisting of three dimensionally linked rod-like segments. *J. Am. Chem. Soc.* **113,** 3606–3607 (1991).
4. Zaworotko, M. J. Cooperative bonding affords a holesome story. *Nature* **386,** 220–221 (1997).
5. Fagan, P. J. & Ward, M. D. Building molecular crystals. *Sci. Am.* **267,** 48–54 (1992).
6. Carlucci, L., Ciani, G., Proserpio, D. M. & Sironi, A. Interpenetrating diamondoid frameworks of silver(I) cations linked by N,N′-bidentate molecular rods. *J. Chem. Soc. Chem. Commun.* 2755–2756 (1994).
7. Mallouk, T. E. Crowns get organized. *Nature* **387,** 350–351 (1997).
8. Gardner, G. B., Venkataraman, D., Moore, J. S. & Lee, S. Spontaneous assembly of a hinged coordination network. *Nature* **374,** 792–795 (1995).
9. Yaghi, O. M., Li, G. & Li, H. Selective binding and removal of guests in a microporous metal-organic framework. *Nature* **378,** 703–706 (1995).
10. Lu, J. *et al.* Coordination polymers of $Co(NCS)_2$ with pyrazine and 4,4-bipyridine: syntheses and structures. *Inorg. Chem.* **36,** 923–928 (1997).
11. Vaid, T. P., Lobkovsky, E. B. & Wolczanski, P. T. Covalent 3- and 2-dimensional titanium-quinone networks. *J. Am. Chem. Soc.* **119,** 8742–8743 (1997).
12. Liu, F. Q. & Tilley, T. D. A coordination network based on d^0 transition-metal centers: synthesis and structure of the [2,4]-connected layered compound $[(TiCl_4)_2Si(C_6H_4CN\text{-}p)4]\cdot 1.5C_7H_8$. *J. Chem. Soc. Chem. Commun.* 103–104 (1998).
13. MacGillivray, L. R., Groeneman, R. H. & Atwood, J. L. Design and self-assembly of cavity-containing rectangular grids. *J. Am. Chem. Soc.* **120,** 2676–2677 (1998).
14. Yaghi, O. M., Li, H., Davis, C., Richardson, D. & Groy, T. L. Synthetic strategies, structure patterns, and emerging properties in the chemistry of modular porous solids. *Acc. Chem. Res.* **31,** 575–585 (1998).
15. Kepert, C. J. & Rosseinsky, M. J. Zeolite-like crystal structure of an empty microporous framework. *J. Chem. Soc. Chem. Commun.* 375–376 (1999).
16. Clegg, W. *et al.* Crystal structures of three basic zinc carboxylates together with infrared and FAB mass spectrometry studies in solution. *Inorg. Chim. Acta* **186,** 51–60 (1991).
17. Harrison, W. T. A. *et al.* Synthesis and characterization of a new family of thermally stable open framework zincophosphate/arsenate phases: $M_3Zn_4O(XO_4)_3\cdot nH_2O$ (M = Na,K,Rb,Li,..; X = P,As; n = ~3.5–6). Crystal structures of $Rb_3Zn_4O(PO_4)\cdot 3.5H_2O$, $K_3Zn_4O(AsO_4)_3\cdot 4H_2O$, and $Na_3Zn_4O(PO_4)_3\cdot 6H_2O$. *Chem. Mater.* **8,** 691–700 (1996).
18. Li, H., Eddaoudi, M., Groy, T. L. & Yaghi, O. M. Establishing microporosity in open metal-organic frameworks: gas sorption isotherms for Zn(BDC) (BDC=1,4-benzenedicarboxylate). *J. Am. Chem. Soc.* **120,** 8571–8672 (1998).
19. Breck, D. W. *Zeolite Molecular Sieves* (Wiley & Sons, New York, 1974).

Supplementary information is available on *Nature*'s World-Wide Web site (http:// www.nature.com) or as paper copy from the London editorial office of *Nature*.

Acknowledgements

We thank F. Hollander and R. Staples for X-ray structure determinations. This work was supported by the National Science Foundation (M.O.K. and O.M.Y.), the Department of Energy (O.M.Y.) and Nalco Chemical Company.

Correspondence and requests for materials should be addressed to O.M.Y. at the University of Michigan (e-mail: oyaghi@umich.edu).

Abrupt termination of the 1997–98 El Niño in response to a Madden–Julian oscillation

Yukari N. Takayabu*, Toshio Iguchi†, Misako Kachi‡, Akira Shibata‡ & Hiroshi Kanzawa*

* *National Institute for Environmental Studies, Tsukuba, Ibaraki, 305-0053, Japan*
† *Communications Research Laboratory, Tokyo, 184-8795, Japan*
‡ *Earth Observation Research Center/NASDA, Tokyo, 106-0032, Japan*

The role of the Madden–Julian oscillation—a global atmospheric wave in the tropics that is associated with convective activity and propagates eastwards with a period of about 30–60 days (refs 1, 2)—in triggering El Niño events has been discussed before[3–8]. But its possible connection with a termination of El Niño has yet to be investigated, despite the difficulty in explaining the timing of El Niño terminations by the basic wind-induced oceanic-wave processes[9,10]. For the extreme 1997–98 event, the mechanism of both onset and termination have been investigated[3], but the reason for the abruptness of the termination has yet to be resolved. Here we present global data of precipitation, sea surface temperatures and wind speeds that show a precipitation system associated with an exceptionally strong Madden–Julian oscilla-